Biosensors and Bioelectronics 29 (2011) 159–166

Contents lists available at ScienceDirect

Biosensors and Bioelectronics

journal homepage: www.elsevier.com/locate/bios

Electrochemical synthesis of reduced graphene sheet–AuPd alloy nanoparticle composites for enzymatic biosensing

Jiang Yang[a], Shengyuan Deng[b], Jianping Lei[b], Huangxian Ju[b,*], Sundaram Gunasekaran[a,**]

[a] Food & Bioproces Engineering Laboratory Department of Biological Systems Engineering, University of Wisconsin-Madison, 460 Henry Mall, Madison, WI 53706, USA
[b] State Key Laboratory of Analytical Chemistry for Life Science, Department of Chemistry, Nanjing University, Nanjing 210093, PR China

ARTICLE INFO

Article history:
Received 10 June 2011
Received in revised form 2 August 2011
Accepted 10 August 2011
Available online 18 August 2011

Keywords:
Biosensor
Electrochemistry
Reduced graphene sheets
Nanoparticles
Metal alloy
Glucose oxidase

ABSTRACT

A simple, fast, green and controllable approach was developed for electrochemical synthesis of a novel nanocomposite of electrochemically reduced graphene oxide (ERGO) and gold–palladium (1:1) bimetallic nanoparticles (AuPdNPs), without the aid of any reducing reagent. The electrochemical reduction efficiently removed oxygen-containing groups in ERGO, which was then modified with homogeneously dispersed AuPdNPs in a good size distribution. ERGO–AuPdNPs nanocomposite showed excellent biocompatibility, enhanced electron transfer kinetics and large electroactive surface area, and were highly sensitive and stable towards oxygen reduction. A biosensor was constructed by immobilizing glucose oxidase as a model enzyme on the nanocomposites for glucose detection through oxygen consumption during the enzymatic reaction. The biosensor had a detection limit of 6.9 μM, a linear range up to 3.5 mM and a sensitivity of 266.6 μA mM^{-1} cm^{-2}. It exhibited acceptable reproducibility and good accuracy with negligible interferences from common oxidizable interfering species. These characteristics make ERGO–AuPdNPs nanocomposite highly suitable for oxidase-based biosensing.

1. Introduction

Heterogeneous bimetallic nanoparticles (NPs) have recently received much attention as electrocatalysts with enhanced activities (Zhang et al., 2007, 2010) and electrochemical reversibility for redox reactions (Katz et al., 2004). These bimetallic alloys can retain the functional properties of each component and possibly offer synergistic effects via cooperative interactions, resulting in important features such as increased surface area, enhanced electrocatalytic activity, improved biocompatibility, promoted electron transfer, and better invulnerability against intermediate species. Pt and Pd are the most frequently used electrocatalysts for oxygen reduction reaction (ORR) with a similar mechanism of $4e^-$ reduction of oxygen to water, while Pd is among the most electrocatalytic metals for ORR besides Pt (Shao, 2011). Since Au is one of the only two transition metals more electronegative than Pt (Zhang et al., 2011b) and is relatively less reactive, the introduction of Au into NPs offers many appealing properties such as biocompatibility (Zhang et al., 2011a), stabilizing effect preventing metal dissolution during ORR (Zhang et al., 2007) and enhanced electrical conductivity (over pure Pd). Gold nanoparticles (AuNPs) in the alloy also act as a biocompatible immobilization matrix necessary for biofunctionalization through ionic interactions and other interactions between AuNPs and mercapto or primary amine groups of biomolecules (Zhang et al., 2011a). Due to the high cost and limited resources of Pt in nature as well as the large miscibility gap between Pt and Au, Pd–Au alloy is an ideal alternative for ORR. The addition of Au to Pd reportedly promotes overall catalytic activity, selectivity, and stability of Pd (Chen et al., 2005). This work developed a simple approach to electrochemically synthesize the bimetallic nanoparticles (AuPdNPs) on electrochemically reduced graphene oxide (ERGO) for probing the application of the Pd–Au alloy in biosensor preparation.

Graphene is a single-atom-thick planar sheet of hexagonally arrayed sp^2-bonded carbon atoms packed in a 2-D honeycomb crystal lattice (Geim and Novoselov, 2007). Many desirable properties of graphene have been revealed such as high surface-to-volume ratio, large surface area, high electrocatalytic activity, fast electron transfer, low cost, robust mechanical properties, flexibility and outstanding conductivity (Stankovich et al., 2006), making it a promising material for applications in electronics/optoelectronics (Muszynski et al., 2008), sensors (Kang et al., 2009; Lu et al., 2011), composites (Stankovich et al., 2006), batteries (Chou et al., 2010) and supercapacitors (Stoller et al., 2008). However, as the existence of residual defects in graphene can exert a significant influence on its electronic properties, efficient reduction of oxygenated

* Corresponding author at: State Key Laboratory of Analytical Chemistry for Life Science, Department of Chemistry, Nanjing University, Nanjing 210093, PR China. Tel.: +1 608 8314862; fax: +86 25 83593593.
** Corresponding author at: Food & Bioproces Engineering Laboratory Department of Biological Systems Engineering, University of Wisconsin-Madison, 460 Henry Mall, Madison, WI 53706, USA. Tel.: +1 608 8314862; fax: +86 25 83593593.
E-mail addresses: hxju@nju.edu.cn (H. Ju), guna@wisc.edu (S. Gunasekaran).

0956-5663/$ – see front matter © 2011 Elsevier B.V. All rights reserved.
doi:10.1016/j.bios.2011.08.011

species in graphene is necessary to prevent possible unwanted reactions and electrostatic adsorptions. Numerous studies have focused on the synthesis and applications of graphene inorganic nanocomposite materials (Lu et al., 2008, 2011; Muszynski et al., 2008). A conductive reduced graphene oxide/Nafion hybrid film via solution chemistry with synergistic effect has been prepared for organophosphate detection (Choi et al., 2010). However, undesirable excessive reducing agents used in these methods both increase the cost in mass production and possibly remain and contaminate the synthesized materials. Meanwhile, oxygen-containing functional groups (–OH, C–O–C in the basal plane and –COOH, C=O on the edges) in graphene cannot be completely eliminated by chemical reduction (Hernandez et al., 2008). Therefore, it is of great interest to look for a simple and environmentally friendly approach for synthesis of graphene sheet-NPs composites.

Electrodeposition is the most controllable and robust technique for synthesis of metal NPs, in which the size, density, composition of alloys and even the shape of NPs can be well-controlled by electrodeposition potential, time, concentration, and composition of metal precursor solutions (Claussen et al., 2009; Yang et al., 2010). Electrochemical methods are also useful in reduction of graphene oxide (GO), strictly speaking an insulator, to eliminate oxygenated defect sites and improve its electronic properties (Guo et al., 2009; Shao et al., 2010). Moreover, the further modification of electrochemically reduced GO with metal NPs can increase its electrical conductivity to a larger extent. Herein, GO was firstly electrochemically reduced on a glassy carbon electrode (GCE) with a process free of reducing agents. The electrochemically synthesized AuPdNPs were then used to modify the ERGO. The as-prepared composite showed enhanced electrocatalytic activity and stability towards O_2 reduction. To demonstrate the significance of the ERGO–AuPdNPs for use in biosensing, GO_x, as a model oxidase, was used to fabricate a sensitive enzymatic biosensor against the clinically important glucose molecule through the consumption of O_2 in the enzymatic reaction. The results showed ERGO–AuPdNPs are a promising material for biosensor preparation, and the as-prepared ERGO–AuPdNPs–GO_x biosensor is an excellent candidate as sensing element for clinical detection of glucose in human blood serum.

2. Materials and methods

2.1. Chemicals and reagents

Graphite powder and D(+)-glucose were purchased from Sinopharm Chemical Reagent, and glucose solution was stored overnight at ambient conditions before use. Uric acid (UA) and L-ascorbic acid (AA) were received from Alfa Aesar. Gold (III) tetrachloride trihydrate ($HAuCl_4{\cdot}3H_2O$), palladium (II) chloride ($PdCl_2$), Nafion, and GO_x (EC 1.1.3.4, type X-S, lyophilized powder, 100–250 units mg^{-1}, from *Aspergillus niger*) were obtained from Sigma–Aldrich. All other reagents were of analytical grade and used as received. Double-distilled Milli-Q water (ddH_2O) (>18.2 MΩ) was used throughout the study and high purity N_2 was applied for deaeration.

2.2. Instruments

Scanning electron microscopy (SEM) and energy dispersive X-ray spectroscopy (EDS) were conducted by EDS-integrated Hitachi S-4800 (Hitachi, Japan) for surface morphology observations and surface elemental composition analysis. Samples for SEM (not EDS) were coated with Au films for increased conductivity using a vacuum spin coater. The particle size distribution was obtained using Image-Pro-Plus software. Atomic force microscopy (AFM) was operated in tapping mode using Agilent 5500 AFM system (Agilent Technologies, USA) with Picoscan software. Static water contact angles were measured with water drops under ambient conditions by Ramé-Hart-100 Contact Angle Goniometer (Ramé-Hart, USA). Cyclic voltammetry (CV) and differential pulse voltammetry (DPV) were performed on a CHI 430A electrochemical analyzer (CH Instruments, USA). All electrochemical measurements were conducted in phosphate buffered saline (0.05 M PBS pH 7.4) unless otherwise specified, on a conventional three-electrode system with a saturated calomel electrode (SCE) as the reference electrode, a Pt wire electrode as the counter electrode and modified glassy carbon electrode as working electrode. Electrochemical impedance spectroscopy (EIS) was carried out using the same three-electrode configuration above on a PGSTAT30/FRA2 system (Autolab, Eco-Chemie, the Netherlands) in a supporting electrolyte solution of 1.0 M KCl containing equimolar $[Fe(CN)_6]^{4-/3-}$ in a frequency range from 0.1 Hz to 100 kHz. The fit and simulation of equivalent circuit were analyzed with FRA software. Roche Modular Chemistry Analyzer (Roche, Switzerland) was used for glucose analysis of human blood serum to compare and validate the performance of the proposed biosensor.

2.3. Synthesis of ERGO

GO was synthesized using a modified Hummer's method (Hummers and Offeman, 1958; Xu et al., 2008). Typically, 3 g graphite powder, 2.5 g $K_2S_2O_8$ and 2.5 g P_2O_5 were added to 12 mL concentrated H_2SO_4 solution and reacted at 80 °C for 4.5 h. After graphite oxidation, the mixture was diluted with 0.5 L water and kept at 80 °C for another 12 h. The resulting solution was then filtered, washed with water and left overnight for drying at room temperature, before re-dispersing in 120 mL concentrated H_2SO_4 with successive addition of 15 g $KMnO_4$ at temperature kept below 20 °C under stirring. The mixture was left stirred at 40 °C for 0.5 h and 90 °C for 1.5 h, followed by dropwise addition of 250 mL water, incubation at 105 °C for 25 min and stirring at room temperature for 2 h. 0.7 L water and 20 mL 30% (w/w) H_2O_2 were added to terminate the reaction. The resulting products were then filtered, washed with 3 M HCl solution, and repeatedly washed with water until the pH value of filtrate was neutral. It was further purified by dialysis for one week to remove residual salts, acids and metal species and was re-suspended by ultrasonication in water to obtain a homogeneous GO solution. GCE was carefully polished on a fine microcloth successively with 0.3 and 0.05 μm alumina slurry (Beuhler) until a mirror-shine surface was obtained, and then rinsed with ddH_2O. A sonication step was performed consecutively in ethanol and ddH_2O and GCE was then dried at room temperature. 3 μL of 1 mg mL^{-1} of the above-prepared GO solution was cast on the pretreated bare GCE surface and dried in ambient condition. The electrochemical reduction of GO on GCE was conducted by repetitive CV scanning from 0 V to −1.5 V at 0.1 V s^{-1} in deaerated 0.05 M pH 5.0 PBS ($NaHPO_4/NaH_2PO_4$) for 100 cycles (Guo et al., 2009). ERGO-modified GCE was then rinsed with water and dried at room temperature.

2.4. Preparation of ERGO–AuPdNPs–GO_x modified GCE

The modification of ERGO with AuPd metal alloy NPs (1:1) was achieved by electrodeposition under a constant potential of −0.2 V in a deaerated precursor solution consisting of 2.5 mM $HAuCl_4$, 2.5 mM $PdCl_2$, and 0.1 M KCl for an optimal time of 100 s. For comparison, ERGO was also modified only by AuNPs or PdNPs, respectively in their corresponding deposition solutions. The ERGO–AuPdNPs–GCE was then rinsed with 0.05 M pH 7.4 PBS, dried at room temperature, and immersed into 0.05 M pH 7.4 PBS containing 2.0 mg mL^{-1} GO_x at 4 °C for 24 h. The resulting ERGO–AuPdNPs–GO_x modified GCE was rinsed several times with

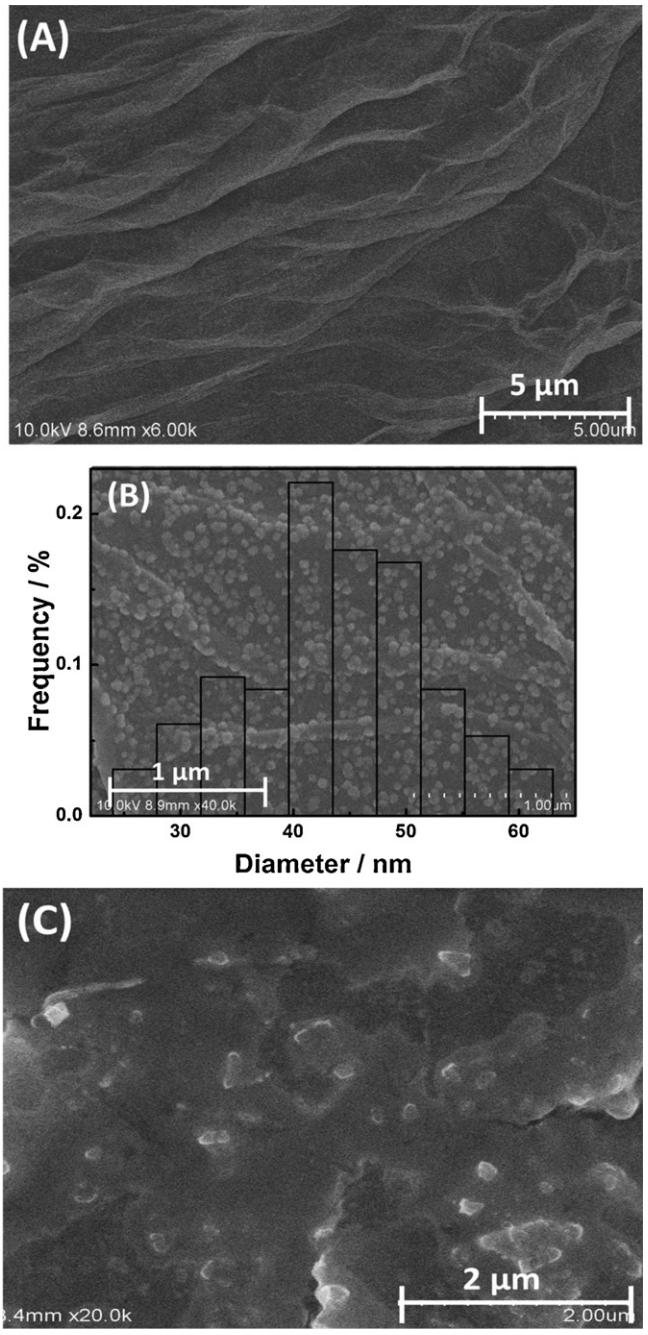

Fig. 1. SEM images of (A) ERGO. (B) AuPdNPs–ERGO. Overlay histogram the particle size distribution of AuPd alloy NPs on the ERGO network. (C) AuPdNPs–ERGO–GO_x.

0.05 M pH 7.4 PBS to wash off loosely absorbed enzyme and 5 μL 1% Nafion was cast on the electrode surface to maintain the stability of biosensor. The electrode was then stored in 0.05 M pH 7.4 PBS at 4 °C ready to use and the glucose detection was done in an electrochemical cell with a flow of N_2 kept on the buffer surface. Indium tin oxide (ITO)-coated glass was modified with the same procedures and used instead of GCE for surface characterization.

3. Results and discussion

3.1. Surface morphology

SEM image of ERGO displayed a typical wrinkled sheet structure of graphene (Fig. 1A). The geometric wrinkling not only minimizes the surface energy but also induces mechanical integrity with high Young's modulus, tensile strength, and good film-forming ability, due to nanoscale sheet interlocking (Xu et al., 2008). The ERGO sheets stacked in parallel provided a large rough surface as scaffold for further modification. After modification, Au–Pd alloy NPs with fairly homogenous diameters of 43.5 ± 8.0 nm were well dispersed in the ERGO network, forming an interpenetrating network for favorable conduction pathways of electron transfer (Fig. 1B). Interestingly, AuPdNPs seemed more prone to deposit in large quantities at ERGO sheets, which were wrinkled or curled into tubular structures and might be attributed to higher static attraction during synthesis, a mechanism similar to that reported for MWCNTs (Yang et al., 2010). After efficiently immobilized in ERGO–AuPdNPs network, GO_x formed a homogenous mushy film with island-like structures, offering an open network for substrate access (Fig. 1C).

The morphology was further analyzed with AFM. The exfoliated, unreduced GO clearly showed flat single layer of graphene nanosheets or multiple layers overlapped together in typical flake-like shape, with fairly smooth surface, with average height between 1 and 2 nm and lateral dimension of around 300 nm, indicating its atomic thickness composition (Fig. 2A). After electrochemical reduction, the average 10–30 nm wrinkled sheets were observed, which proved that the electrochemical reduction of GO was successful. Noticeably, some ERGO sheets were even wrinkled and curled into tubular-like structures, further increasing roughness and surface area. Electrochemical reduction was presumed to cause the observed restacking, corrugation and crumpling of GO sheets and therefore provided a good membrane-forming ability with larger surface coverage on substrate, suitable for large-scale production of reduced graphene sheets. When ERGO was further modified with AuPdNPs, the height profile obviously became rougher to a greater extent (Fig. 2C), with more electroactive sites and larger surface area. The height measurement showed AuPdNPs had diameters between 20 and 50 nm, consistent with the particle size distribution data (Fig. 1B). As GO_x was immobilized, a fairly smooth film formed with clear island-like structures and small cracks (Fig. 2D), providing a good platform for biosensing.

3.2. Characterizations of ERGO–AuPdNPs nanocomposites

Elemental compositions of ERGO–AuPdNPs were analyzed by EDS (Fig. 3A). Signature peaks for C, Au and Pd were observed for ERGO–AuPdNPs, while all other elements were from ITO substrates. The weight percentage of Au and Pd in the alloy NPs was 64.9% and 35.1% respectively, resulting in an atomic ratio close to 1:1. This corresponded well to the molar ratio of metal precursors and indicated Au and Pd can both be successfully electrochemically synthesized under the given conditions and contribute equally towards formation of bimetallic NPs during the synthesis.

The hydrophilicity, measured quantitatively by contact angles, is indicative of biocompatibility of materials (Deng et al., 2009). The contact angle of unreduced GO (40.0°) was smaller than that of ITO glass substrate (66.7°) (Fig. 3B), suggesting unreduced GO is fairly hydrophilic due to abundance of oxygen-containing functional groups. When GO was electrochemically reduced, the resulting ERGO became hydrophobic with an increased contact angle of 72.4°, indicating the elimination of oxygenated species. After modification of AuPdNPs, the contact angle of ERGO–AuPdNPs decreased to 41.8°, retaining a hydrophilicity comparable to that of unreduced GO, which is hydrophilic. The biocompatibility of ERGO–AuPdNPs nanocomposites could significantly facilitate enzyme immobilization with preserved bioactivity of the enzymes.

EIS is a useful tool to monitor modifications step-by-step using $[Fe(CN)_6]^{4-/3-}$ redox couple as electrochemical probe (Fig. 3C). As GCE was modified with ERGO (curve b), the charge transfer resistance (R_{ct}) drastically decreased compared to that of bare GCE

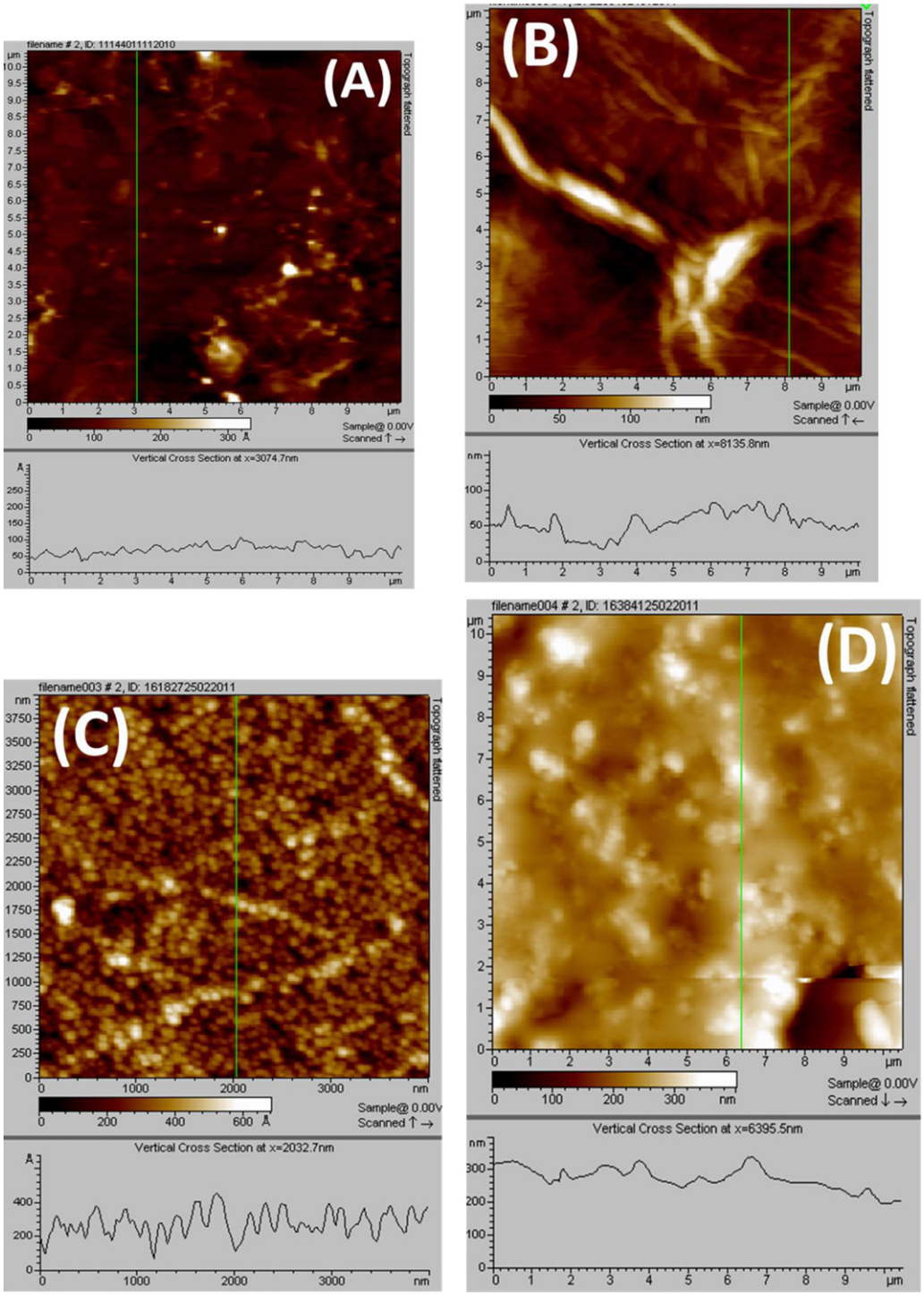

Fig. 2. AFM images with height profiles along the marked lines of (A) GO, (B) ERGO, (C) ERGO–AuPdNPs, (D) ERGO–AuPdNPs–GO_x.

(curve a). This implied ERGO formed an interpenetrating network in favor of diffusion of redox probes and interfacial electron transfers. R_{ct} continued to decrease as ERGO was further modified with metal NPs, at 49.0, 108.9 and 39.6 Ω for Au, Pd and AuPd NPs respectively (curve c, d, e). This result showed AuPd alloy NPs were better electron-transfer interface between electrode surface and electrolyte solution and also between electroactive sites of immobilized enzyme and electrode, compared to pure metal NPs, making ERGO–AuPdNPs an ideal platform for biosensors. With GO_x successfully immobilized, R_{ct} of ERGO–AuPdNPs–GO_x (curve f) dramatically increased to beyond 10 kΩ, due to the blocking effects of GO_x on electron transfer.

3.3. Electrochemical characterizations of ERGO–AuPdNPs

The repetitive cyclic voltammograms (100 cycles) for electrochemical reduction of GO modified GCE were shown in Fig. 4A. An overwhelming cathodic reduction current starting from −0.7 V up to −1.5 V was found in the first cycle, with a current peak around −1.3 V, which was ascribed to reduction of surface oxygen groups.

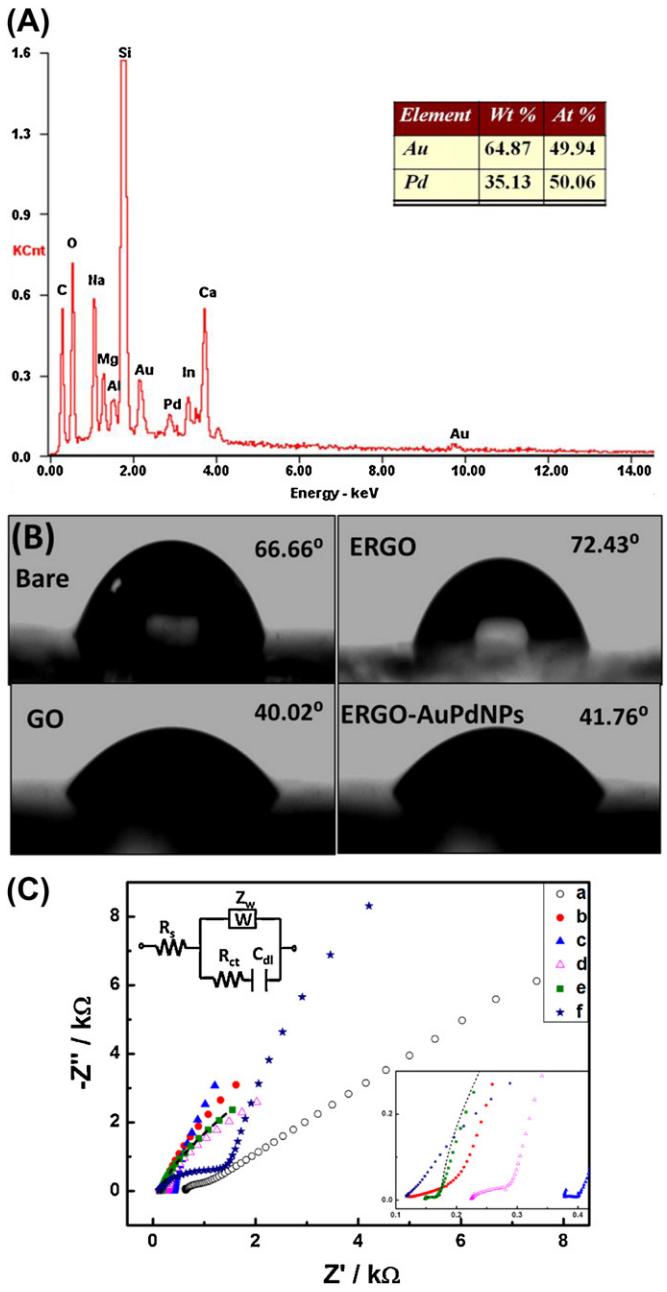

Fig. 3. (A) EDS spectra of AuPdNPs–ERGO. Inset shows the weight and atomic percentages of Au and Pd in the alloy. (B) Contact angles of bare, GO, ERGO and ERGO–AuPdNPs on substrates. (C) EIS spectra of (a) bare, (b) ERGO, (c) ERGO–AuNPs, (d) ERGO–PdNPs, (e) ERGO–AuPdNPs, (f) ERGO–AuPdNPs–GO_x modified GCEs in 1.0 M KCl containing 5.0 mM $K_4[Fe(CN)_6]/K_3[Fe(CN)_6]$. Lower right inset shows magnification of the high frequency region. The dotted line indicates the simulation result of equivalent circuit $R_s([R_{ct}C_{dl}]Z_w)$ on the upper left to fit ERGO–AuPdNPs. R_s: solution resistance, R_{ct}: electron transfer resistance, C_{dl}: double layer capacitance, Z_w: Warburg impedance.

This result was similar to that reported previously (Guo et al., 2009), with a very close peak current. The reduction current began to drop exceptionally in the second cycle and continued to decrease with the CV scans progressing until it was not noticeable. After only a few potential sweeps, the reduction current disappeared in later cycles and the baseline current reached a stable plateau, manifesting the surface-oxygenated species were successfully reduced in a rapid way. After electrochemical reduction, the formed ERGO became black, which could be more clearly seen on ITO.

At ERGO modified GCE the cyclic voltammogram of 5.0 mM $K_3[Fe(CN)_6]$ in 1.0 M KCl showed a slightly smaller peak potential separation and larger peak current (Fig. 4B, curve b) than that at bare GCE (curve *a*), demonstrating faster electron transfer and larger electroactive surface area for ERGO. After modification with metal NPs, peak potential separations (curve *d*, 89 mV @ Pd; curve *c*, 69 mV @ Au; curve *e*, 65 mV @ AuPd) decreased while peak current (AuPd > Au ≈ Pd) increased. The marked increase in the current of ERGO–AuPdNPs compared to that in ERGO confirmed the contribution of AuPdNPs in increasing the electroactive surface area and promotion of electron transfers. When GO_x was immobilized (curve f), the peak current went down dramatically. The peak separation increased considerably to more than 300 mV. These were caused by the large GO_x protein molecules, which blocked electron transfers at the interface. Notably, ERGO–AuPdNPs modified electrode showed a peak separation value very close to the ideal kinetics (59 mV) of one-electron reversible process, revealing excellent conductivity and ideal reversibility of the redox reaction. The effective surface area of ERGO, ERGO–AuPdNPs and ERGO–AuPdNPs–GO_x can be calculated by Randles–Sevcik equation to be 0.067 ± 0.002, 0.081 ± 0.002 and $0.017 \pm 0.003\ cm^2$, respectively.

3.4. Electrocatalytic performance of ERGO–AuPdNPs–GO_x biosensor

The electrocatalysis of O_2 reduction was investigated by CV in 0.05 M pH 7.4 PBS at $0.1\ V\ s^{-1}$ (Fig. 4C). In N_2-saturated PBS, AuPdNPs modified GCE did not show any significant peak (curve e) while ERGO modified GCE displayed a pair of weak and broad redox peaks with cathodic peak lying between −0.4 V and −0.3 V and anodic peak at around −0.2 V (curve b), due to subtle incomplete electrochemical reduction of oxygen species. In fact, most unstable oxygen-containing groups in ERGO (as the high cathodic current in Fig. 4A) have been reduced or eliminated with very weak redox peaks observed, while the remaining unreduced ones are only a small portion which might have been electrochemically stabilized during the extensive CV cycling, with little damage on its electrical properties (Shao et al., 2010). As for ERGO–AuPdNPs modified GCE, it retained the minor redox peaks from ERGO in a nearly rectangular shape, interpreting good electron propagation within the electrode (curve d). On the other hand, in air-saturated PBS, ERGO modified GCE exhibited negligible current response towards O_2 (curve a). In contrast, both AuPdNPs (curve f) and ERGO–AuPdNPs (curve c) modified GCEs yielded a significant current increase, with onset potential of −0.05 V for AuPdNPs and +0.1 V for ERGO–AuPdNPs. Therefore, AuPd metal alloy NPs of ERGO–AuPdNPs nanocomposites play the key role in ORR. Moreover, the onset potential of ORR for ERGO–AuPdNPs is more positive than N-doped graphene (−0.2 V) (Qu et al., 2010), N-doped MWCNT arrays (−0.05 V) (Gong et al., 2009) and porous carbon–tetrathiafulvalene composites (−0.05 V) (Ndamanisha et al., 2010). Apparently, the current response of ERGO–AuPdNPs against O_2 was much higher than that of AuPdNPs and the peak potential of oxygen reduction at ERGO–AuPdNPs was −0.05 V compared to that of AuPdNPs at −0.2 V. The obviously low cathodic overpotential of ORR demonstrated a higher electrocatalytic activity of ERGO–AuPdNPs. This superior O_2 electrocatalytic performance of ERGO–AuPdNPs over AuPdNPs was attributed to the larger surface area, more electroactive sites, faster electron transfer kinetics and the interpenetrating low-resistance 2-D network of ERGO, favorable for dispersion and nucleation of AuPdNPs. Also, given its relatively simple and environment-friendly synthesis, ERGO–AuPdNPs has the potential to be an excellent material for ORR.

Based on the consumption of oxygen in the enzymatic reaction with glucose and the enormously enhanced catalytic activity of ERGO–AuPdNPs nanocomposites towards oxygen reduction, an

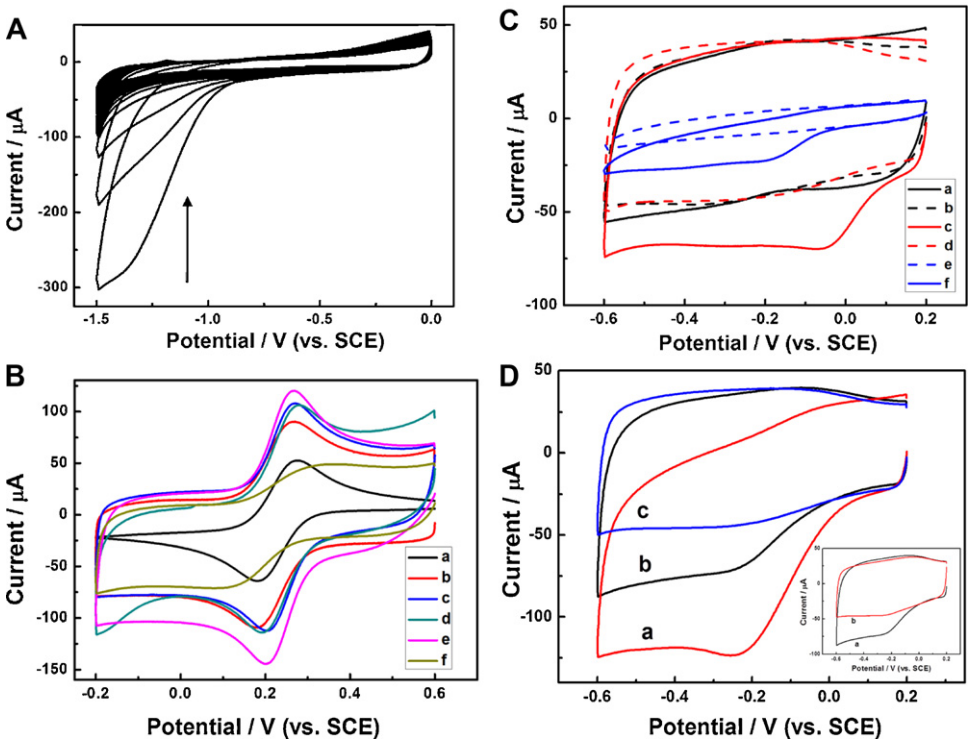

Fig. 4. Cyclic voltammograms of (A) GO-modified GCE in deaerated 0.05 M pH 5.0 PBS (100 cycles starting at −1.5 V). The big arrow indicates the progression of potential scanning while the small one denotes the reduction peak of GO. (B) (a) Bare, (b) ERGO, (c) ERGO–AuNPs, (d) ERGO–PdNPs, (e) ERGO–AuPdNPs, (f) ERGO–AuPdNPs–GO_x modified GCEs in 5.0 mM $K_3[Fe(CN)_6]$ + 1.0 M KCl. (C) (a and b) ERGO (black), (c and d) ERGO–AuPdNPs (red), (e and f) AuPdNPs (blue) modified GCEs in 0.05 M pH 7.4 PBS saturated with (a, c and f) air (solid lines) and (b, d and e) N_2 (dotted lines). (D) ERGO–AuPdNPs–GO_x modified GCE in 0.05 M pH 7.4 PBS saturated with (a) O_2, (b) air and (c) N_2. Inset shows ERGO–AuPdNPs–GO_x modified GCE in air-saturated 0.05 M pH 7.4 PBS in the absence (a) and presence (b) of 3.0 mM Glc. Scan rates for all figures: 0.1 V s^{-1}. (For interpretation of the references to color in this figure legend, the reader is referred to the web version of the article.)

enzymatic biosensor was fabricated by immobilizing GO_x into ERGO–AuPdNPs network. Glucose concentration could therefore be monitored by decrease in cathodic current signal from ORR. After GO_x immobilization, ERGO–AuPdNPs–GO_x exhibited a higher cathodic current in air-saturated PBS (curve b) than in N_2-saturated PBS (curve c), proving it preserved the electrocatalytic activity of ERGO–AuPdNPs towards O_2 (Fig. 4D). This was further confirmed by the observation of a much more remarkable current increase in O_2-saturated PBS (curve a) than air-saturated PBS. The cathodic peak potential of ERGO–AuPdNPs–GO_x shifted from −0.05 V at ERGO–AuPdNPs to around −0.2 V, accompanied by diminishing peak current, which was triggered by the enzyme film. In the air-saturated PBS solution with 3.0 mM glucose, an obvious peak current decrease of ORR due to consumption of O_2 was seen (Fig. 4D inset), which could be used, in combination with the good selectivity of GO_x, for determination of glucose.

Different durations of electrodeposition could lead to different densities, sizes, and even shapes of NPs formed on ERGO, resulting in varied catalytic activities against O_2 reduction. The effect of deposition time on electrocatalytic activity of O_2 reduction at ERGO–AuPdNPs modified GCE was shown in Fig. 5A. The highest electrocatalysis of O_2 was achieved at 100 s. At shorter deposition time, the electroactive sites on ERGO surface could not be entirely occupied and AuPdNPs could not efficiently nucleate, causing a low density of NP dispersion, less electrocatalytic sites and thereby a low sensitivity against O_2 reduction. However, longer time would cause NPs to aggregate into larger particles or bulk clusters, eliminating the advantage of NPs with larger reactive surface area. Furthermore, the electrocatalytic activity of bimetallic ERGO–AuPdNPs was also compared with ERGO–AuNPs and ERGO–PdNPs (Fig. 5A inset). It was observed that ERGO–AuNPs could achieve about 70% the electrocatalytic activity of ERGO–AuPdNPs, whereas ERGO–PdNPs had a lower electrocatalytic activity than ERGO–AuPdNPs. It should be noted that being a strong catalyst, Pd showed astonishingly superior initial performance in O_2 reduction, however it could not be sustained. This decrease in catalytic performance is due to gradual dissolution of Pd and its vulnerability towards intermediate species (Zhang et al., 2010). Therefore, introduction of Au in Pd could both enhance the catalytic activity and stability against O_2, owing to the isolation of single Pd sites by Au, which could facilitate the coupling of surface species (Chen et al., 2005).

Glucose determination was accomplished by DPV in air-saturated 0.05 M pH 7.4 PBS (Fig. 5B). When glucose was absent, only one peak between −0.1 and −0.2 V, which ascribed to O_2 reduction at ERGO–AuPdNPs–GO_x, was found, without any other peaks interfering the detection. Upon glucose addition, the current of the peak began to decrease, with a linear dependence on glucose concentration in the range of 0.5–3.5 mM (R^2 = 0.99). With increasing glucose concentration, the weak and unnoticeable peak from ERGO at around −0.3 V began to become noticeable (relatively obvious for DPV with addition of 3.5 mM glucose and higher), though it did not hinder the detection. Based on the calibration curve, the sensitivity of the biosensor was calculated to be 266.6 μA mM^{-1} cm^{-2} (Fig. 5B inset), with a detection limit of 6.9 μM at signal/noise ratio of 3. This sensitivity was higher than that reported for many enzymatic sensors such as 5.2 μA mM^{-1} cm^{-2} for GO_x/Pd–Au/ASWCNTs/Si (Claussen et al., 2009), 13.0 μA mM^{-1} cm^{-2} for N doped-MWCNTs-GO_x (Deng et al., 2009), 37.9 μA mM^{-1} cm^{-2} for GO_x–graphene–chitosan (Kang et al., 2009), 61.5 μA mM^{-1} cm^{-2} and 47.9 μA mM^{-1} cm^{-2} for Pt or PdNPs–*x*GnPs–GO_x (Lu et al., 2008) as well as non-enzymatic ones

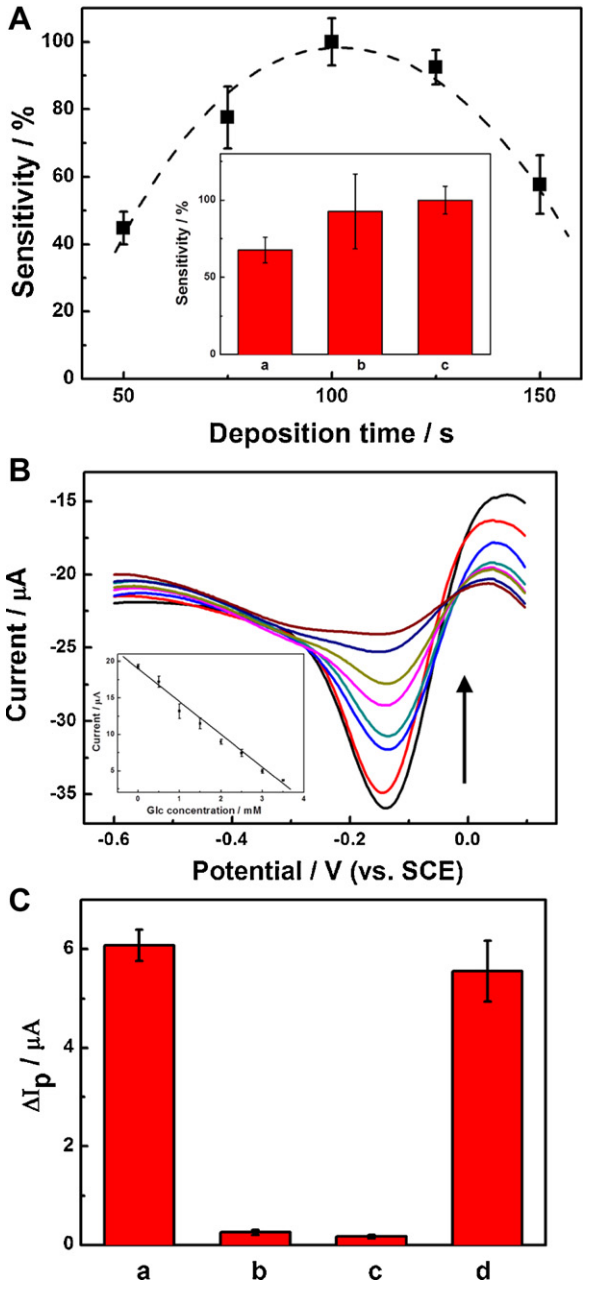

Fig. 5. (A) Effect of deposition time on sensitivity against O_2. Inset shows sensitivities of (a) ERGO–AuNPs, (b) ERGO–PdNPs, (c) ERGO–AuPdNPs modified GCEs against O_2. (B) Differential pulse voltammograms of ERGO–AuPdNPs–GO_x modified GCE in air-saturated 0.05 M pH 7.4 PBS containing 0.0–3.5 mM Glc from outside to inside as the arrow indicates, at a potential step of 4 mV, a frequency of 60 Hz and amplitude of 50 mV. Inset shows linear dependence of peak currents on Glc concentrations as calibration curve. (C) Peak current decreases of DPV at ERGO–AuPdNPs–GO_x modified GCE in air-saturated 0.05 M pH 7.4 PBS in the presence of (a) 1.0 mM Glc, (b) 1.0 mM AA, (c) 1.0 mM UA and (d) 1.0 mM Glc after being stored for two weeks. Error bars indicate standard deviations of triplicate measurements.

such as 160.0 μA mM^{-1} cm^{-2} at PdNPs-SWNTs (Meng et al., 2009) and 10.8 μA mM^{-1} cm^{-2} at nanoporous PtPb (Wang et al., 2008). The indicator of enzyme–substrate reaction kinetics, the apparent Michaelis–Menten constant (K_m^{app}), was calculated according to the electrochemical version of Lineweaver–Burk equation to be 10.5 mM, presenting a good substrate affinity towards glucose.

Table 1
Comparison of glucose concentrations ($n = 3$) in human blood serum samples measured by the proposed biosensor and a clinical chemistry analyzer.

Serum sample	The proposed biosensor (mM)	Roche modular system (mM)	Recovery rate (%)
1	7.56 ± 0.48	8.07	93.2
2	5.86 ± 0.55	5.27	95.7
3	4.37 ± 0.43	4.86	108.0
4	8.22 ± 0.36	8.50	101.5

3.5. Analytical applications of ERGO–AuPdNPs–GO_x biosensor

The influence of oxidizable interfering species possibly coexisting with glucose in human blood serum was examined by investigating the ORR peak current change of DPV with 1.0 mM UA or AA added to 1.0 mM glucose in air-saturated 0.05 M pH 7.4 PBS (Fig. 5C). There was only a minimal interference of 4.2% and 2.9% from AA and UA respectively to glucose, without appearance of any additional peak. A good selectivity against endogenously coexisting electroactive species was presented by ERGO–AuPdNPs–GO_x biosensor (Wang et al., 2008), due to the low overpotential at which these species generate negligible response. The stability was tested by measuring the peak current decrease of ORR against 1.0 mM glucose (Fig. 5C, d) with the biosensor stored in 0.05 M pH 7.4 PBS at 4 °C. There was no significant decrease in response in several days and only an 8.6% loss of original response was observed after two weeks of storage, implying that the enzyme was stably immobilized in ERGO–AuPdNPs network with its bioactivity well preserved. The reproducibility of the biosensor was checked by detecting 1.0 mM glucose using five independently fabricated electrode, with an acceptable relative standard deviation (RSD) of 9.7%, while 10 successive measurements of 1.0 mM glucose were conducted at the same electrode with a RSD of 6.3%.

The performance of the biosensor was tested by measuring Glucose concentration in human blood serum samples obtained from hospital, and the results were compared with those measured with a clinical Roche Modular Chemistry Analyzer (Table 1). Serum samples of four individuals were drawn and tested without any pretreatments. The normal glucose concentration in human serum is in the range of 3.0–8.0 mM, while in serum of some diabetic patients it can reach as high as 13.0 mM. Limited by the comparative narrow linear range of the proposed biosensor, which only has an upper limit of 3.5 mM, the serum samples were diluted before testing. The results from the biosensor were similar (±10%) to those obtained by the clinical analyzer. The recovery rates of the biosensor were estimated to be over 90%, validating its suitability as a novel nanocomposite material for routine glucose measurements. Our future work will optimize the biosensor performance in detecting glucose by varying the atomic ratio of metals, doping additional metals in the alloys, introducing biopolymer membranes to increase biocompatibility, as well as application of other oxidases.

4. Conclusions

A simple, controllable, fast, convenient and green electrochemical approach is proposed to synthesize reduced GO–AuPdNPs nanocomposites in which oxygenated species are efficiently removed without any reducing agent. The synthesized ERGO–AuPdNPs composite shows a homogeneous dispersion of the Au–Pd alloy NPs in the wrinkled ERGO scaffold, with good biocompatibility, fast electron transfer kinetics, large electroactive surface area, high sensitivity and stability against O_2 reduction. Based on these appealing characteristics, a glucose biosensor can be fabricated by detecting the O_2 consumption during the

enzymatic reaction of GO_x. The as-prepared biosensor exhibits a high sensitivity, good stability, acceptable reproducibility, high substrate affinity and specificity in glucose detection and can be successfully applied in clinical detection of glucose in human serum, affording a new approach for developing oxidase-based biosensors.

Acknowledgements

We acknowledge World Universities Network grant for funding and Jiangsu Institute of Cancer Prevention and Cure, Nanjing, China for human blood serum test samples and clinical services.

References

Chen, M., Kumar, D., Yi, C.-W., Goodman, D.W., 2005. Science 310, 291–293.
Choi, B.G., Park, H., Park, T.J., Yang, M.H., Kim, J.S., Jang, S.-Y., Heo, N.S., Lee, S.Y., Kong, J., Hong, W.H., 2010. ACS Nano 4, 2910–2918.
Chou, S.-L., Wang, J.-Z., Choucair, M., Liu, H.-K., Stride, J.A., Dou, S.-X., 2010. Electrochem. Commun. 12, 303–306.
Claussen, J.C., Franklin, A.D., ul Haque, A., Porterfield, D.M., Fisher, T.S., 2009. ACS Nano 3, 37–44.
Deng, S., Jian, G., Lei, J., Hu, Z., Ju, H., 2009. Biosens. Bioelectron. 25, 373–377.
Geim, A.K, Novoselov, K.S., 2007. Nat. Mater. 6, 183–191.
Gong, K., Du, F., Xia, Z., Durstock, M., Dai, L., 2009. Science 323, 760–764.
Guo, H.-L., Wang, X.-F., Qian, Q.-Y., Wang, F.-B., Xia, X.-H., 2009. ACS Nano 3, 2653–2659.
Hernandez, Y., Nicolosi, V., Lotya, M., Blighe, F.M., Sun, Z., De, S., McGovern, I.T., Holland, B., Byrne, M., Gun'Ko, Y.K., Boland, J.J., Niraj, P., Duesberg, G., Krishnamurthy, S., Goodhue, R., Hutchison, J., Scardaci, V., Ferrari, A.C., Coleman, J.N., 2008. Nat. Nano 3, 563–568.
Hummers, W.S., Offeman, R.E., 1958. J. Am. Chem. Soc. 80, 1339.
Kang, X., Wang, J., Wu, H., Aksay, I.A., Liu, J., Lin, Y., 2009. Biosens. Bioelectron. 25, 901–905.
Katz, E., Willner, I., Wang, J., 2004. Electroanalysis 16, 19–44.
Lu, J., Do, I., Drzal, L.T., Worden, R.M., Lee, I., 2008. ACS Nano 2, 1825–1832.
Lu, L.-M., Li, H.-B., Qu, F., Zhang, X.-B., Shen, G.-L., Yu, R.-Q., 2011. Biosens. Bioelectron. 26, 3500–3504.
Meng, L., Jin, J., Yang, G., Lu, T., Zhang, H., Cai, C., 2009. Anal. Chem. 81, 7271–7280.
Muszynski, R., Seger, B., Kamat, P.V., 2008. J. Phys. Chem. C 112, 5263–5266.
Ndamanisha, J.C., Bo, X., Guo, L., 2010. Analyst 135, 621–629.
Qu, L., Liu, Y., Baek, J.-B., Dai, L., 2010. ACS Nano 4, 1321–1326.
Shao, M., 2011. J. Power Sources 196, 2433–2444.
Shao, Y., Wang, J., Engelhard, M., Wang, C., Lin, Y., 2010. J. Mater. Chem. 20, 743–748.
Stankovich, S., Dikin, D.A., Dommett, G.H.B., Kohlhaas, K.M., Zimney, E.J., Stach, E.A., Piner, R.D., Nguyen, S.T., Ruoff, R.S., 2006. Nature 442, 282–286.
Stoller, M.D., Park, S., Zhu, Y., An, J., Ruoff, R.S., 2008. Nano Lett. 8, 3498–3502.
Wang, J., Thomas, D.F., Chen, A., 2008. Anal. Chem. 80, 997–1004.
Xu, Y., Bai, H., Lu, G., Li, C., Shi, G., 2008. J. Am. Chem. Soc. 130, 5856–5857.
Yang, J., Zhang, W.-D., Gunasekaran, S., 2010. Biosens. Bioelectron. 26, 279–284.
Zhang, J., Lei, J., Pan, R., Leng, C., Hu, Z., Ju, H., 2011a. Chem. Commun. 47, 668–670.
Zhang, J., Sasaki, K., Sutter, E., Adzic, R.R., 2007. Science 315, 220–222.
Zhang, S., Shao, Y., Liao, H.-g., Liu, J., Aksay, I.A., Yin, G., Lin, Y., 2011b. Chem. Mater. 23, 1079–1081.
Zhang, S., Shao, Y., Yin, G., Lin, Y., 2010. Angew. Chem. Int. Ed. 49, 2211–2214.